Northumbria Research Link

Northumbria University NEWCASTLE

UniversityLibrary

An energy-balance model for debris-covered glaciers including heat conduction through the debris layer

Tim D. REID, Ben W. BROCK

School of Social and Environmental Sciences, University of Dundee,
Dundee DD1 4HN, UK
E-mail: t.d.reid@dundee.ac.uk

ABSTRACT. Extensive covers of supraglacial debris are often present in glacier ablation areas, and it is essential to assess exactly how the debris affects glacier melt rates. This paper presents a physically based energy-balance model for the surface of a debris-covered glacier. The model is driven by meteorological variables, and was developed using data collected at Miage glacier, Italy, during the ablation seasons of 2005, 2006 and 2007. The debris surface temperature is numerically estimated by considering the balance of heat fluxes at the air/debris interface, and heat conduction through the debris is calculated in order to estimate melt rates at the debris/ice interface. The predicted hourly debris surface temperatures and debris internal temperatures provide a good fit to temperatures measured on rock-covered Miage glacier ($r^2 > 0.94$) and the tephra-covered glacier on Villarrica volcano, Chile ($r^2 > 0.82$). The model can also be used to reproduce observed changes in melt rates below debris layers of varying types and thicknesses, an important consideration for the overall mass balance of debris-covered glaciers.

INTRODUCTION

Many glacier ablation zones are mantled in near-continuous blankets of rock debris. These debris-covered glaciers are important components of the water cycle in many mountain regions (e.g. in the headwaters of the Ganges and Indus rivers). The extent of glacial debris covers has been seen to expand in recent decades in major mountain ranges including the European Alps (e.g. Kellerer-Pirklbauer, 2008), the Caucasus (e.g. Popovnin and Rozova, 2002; Stokes and others, 2007), the Himalaya (e.g. Bolch and others, 2008; Shukla and others, 2009) and the Southern Alps of New Zealand (e.g. Kirkbride, 1993). The debris layers have a very significant impact on glacier thermo-dynamics (Brock and others, 2010), so it is essential to assess exactly how their presence affects glacier responses to atmospheric changes. However, while many studies have investigated the surface energy balance on clean or debris-free glaciers, there is still a lack of models of the processes that influence debris-covered snow and ice. This paper presents a physically based, one-dimensional melt model named the DEB model (debris energy-balance model) for a debris-covered glacier. The model is driven by meteoro-logical variables and specified debris thermal properties, and calculates surface temperatures and melt rates similar to measurements taken at the rock-debris-covered Miage glacier, Italy, and a tephra-covered glacier on Villarrica volcano, Chile, for various values of debris thickness. A statistical analysis of the model is presented which highlights the most important model variables and processes, and provides insight into the effects of debris thermal properties. We also present a theoretical discussion of how such a model could imitate the well-known 'Østrem curve' (Østrem, 1959) – which shows that thin debris enhances melt, while thicker debris covers reduce melt – by simulating a situation where thinner debris covers grow more 'patchy', with exposed portions of ice increasing the surface albedo.

DATA USED FOR MODELLING

The majority of data used to develop the DEB model were collected using an automatic weather station (AWS) located at 2030 m a.s.l. on the lower debris-covered ablation zone of Miage glacier (45°47′ N, 06°52′ E). The data-collection regime is fully described by Brock and others (2010). The variables used in this paper are:

$S\downarrow$	Incoming shortwave radiation (W m^{-2})
$S\uparrow$	Reflected shortwave radiation (W m^{-2})
$L\downarrow$	Downwelling longwave radiation (W m^{-2})
$L\uparrow$	Upwelling longwave radiation (W m^{-2})
T_a	Air temperature at 2.16 m height (K)
u	Wind speed at 2.16 m height (m s^{-1})
RH_a	Relative humidity in air at 2.16 m height (%)
RH_s	Relative humidity at debris surface (%)
T_s	Debris surface temperature (K)

Data for the above variables were collected on an hourly basis for the majority of the ablation seasons in 2005, 2006 and 2007. Although collection dates differed slightly between years, complete blocks of hourly data were collected between 0100 h on 21 June and 2400 h on 4 September in all three years. These blocks, each repre-senting 76 full days or 1824 hourly data points, were used in this study in order to have direct comparisons between the same dates in different years. The only variable with considerable gaps due to sensor failure over this period was surface relative humidity, RH_s, which was not collected from 0700 h on 23 July to 0800 h on 28 July inclusively in 2005 (122 missing data points), was not collected at all in 2006 and was available only for sporadic periods in 2007 (1291 missing data points). This paper also makes use of tempera-ture and precipitation data from the Lex Blanche meteoro-logical station, located ~4 km from Miage glacier at 2162 m, and meteorological and debris data collected on the glacier of Villarrica volcano, Chile (Brock and others, 2007).
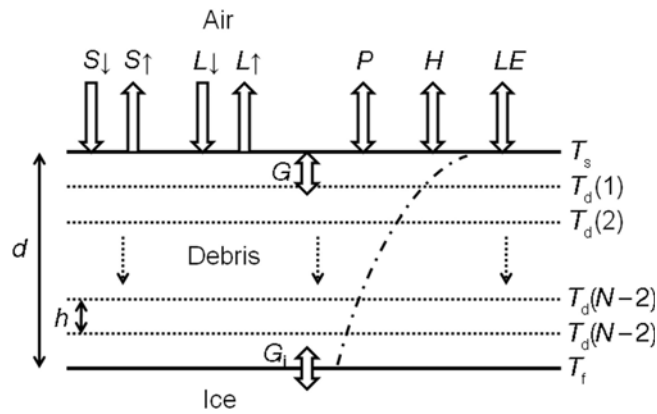
Fig. 1. Schematic of the DEB model showing heat fluxes at the top and bottom of a debris layer of thickness d. The debris temperature is calculated for N layers of thickness h, with boundary conditions defined by the surface temperature, T_s, and the temperature of the debris/ice interface, which is assumed to stay at $T_f = 0°C$. The dash–dot curve is an example temperature profile, where temperature increases towards the right.

ENERGY-BALANCE MODELS

Energy-balance models (EBMs) have been developed for both debris-covered glaciers (e.g. Nakawo and Young, 1981; Nicholson and Benn, 2006) and 'clean' glaciers (e.g. Hay and Fitzharris, 1988; Arnold and others, 1996; Brock and Arnold, 2000; Klok and Oerlemans, 2002; Pellicciotti and others, 2008), using a general form determined by the sum of fluxes at the atmosphere/glacier boundary. For example:

$$M = S + L + H + LE + P + G, \tag{1}$$

where M is the energy available for melt, S is net solar shortwave radiation, L is net longwave radiation, H is sensible heat transfer, LE is latent heat transfer, P is the heat flux due to precipitation and G is the conductive heat flux below the surface. The drawback to EBMs is that the flux calculations depend on quantities such as surface temperature, surface humidity and internal debris temperatures, which are not regularly measured on or near glacier sites. More importantly, such variables are not predicted to sufficiently high resolution by the global or regional-scale climate models that should be applied for future projections of glacial activity. For this reason, many studies have made use of 'temperature-index' or 'degree-day' models (e.g. Mihalcea and others, 2006), which rely on a simple empirical correlation between air temperature and melt, or enhanced temperature-index (ETI) models that work via a regression of melt rate with air temperature and solar shortwave radiation (Pellicciotti and others, 2005). However, in a study comparing melt models of different complexity, Pellicciotti and others (2008) point out that ETI models are limited by being calibrated for a glacier with specific climatic and topographic conditions and cannot necessarily be applied to different regions. This is exacerbated for debris-covered glaciers, due to variations in debris layer structure, thickness and lithology. There may therefore be benefits in finding models that are as generalizable as an EBM but require fewer input variables and parameters. Another concern is that, while the long-term predictions of melt models can be compared to manual stake measurements taken a few times during an ablation season, model accuracy could be considerably improved by testing the

short-term performance of a model against higher-resolution data, for example to check that the model picks up on sudden anomalous melt events. In this paper, we identify the debris surface temperature, T_s, as a useful variable for model testing. T_s and internal debris temperatures, T_d, are treated as unknowns that are calculated alongside the heat fluxes. This presents something of a circularity problem, namely that T_s and T_d not only depend on the surface fluxes, but are also required for the calculation of the fluxes. In the DEB model, this problem is solved by using numerical algorithms. A similar approach for calculating T_s was used by Nicholson and Benn (2006), predicting surface temperatures and melt rates very similar to data. However, their model was tested over periods of just 4–11 days, did not take account of atmospheric stability and did not fully simulate heat conduction through the debris layer. Instead, they assumed that, provided a minimum model time-step of 24 hours is used, the temperature gradient throughout the debris layer can be considered linear (having been informed by measurements showing that, although the profile is nonlinear at various times throughout the day, it is approximately linear on a 24 hour averaged basis). Brock and others (2010) also assume a linear temperature profile, but use a 1 hour time-step, and introduce a 'debris heat storage' flux to account for debris warming during the day and cooling at night. In reality, the assumption of a linear profile may lead to inaccuracies, especially if one considers that the most nonlinear temperature profiles tend to occur due to surface heating during the day, when most melt occurs. It is useful to explicitly model such processes in as much detail as possible, before using model validation and statistical analysis procedures to assess whether they can be simplified. The long-term, high-resolution data collected on Miage glacier present an excellent opportunity for this. The processes simulated in the DEB model are illustrated in Figure 1. Our methods make it possible to assess model performance by comparing the model-calculated T_s to data at a high temporal resolution.

Debris surface temperature

The air/debris interface temperature, T_s, is considered to change on every time-step to a temperature which will cause the sum of heat fluxes at the debris surface to be zero, to obey laws of conservation of energy. Given that some of the fluxes are functions of T_s while some are not, we can write:

$$S + L\downarrow + L\uparrow (T_s) + H(T_s) + LE(T_s) + G(T_s) + P(T_s) = 0$$
$$\text{or simply: } F(T_s) = 0. \tag{2}$$

Launiainen and Cheng (1998), Nicholson and Benn (2006), Reid and Crout (2008) and Van den Broeke and others (2008) report using numerical methods to solve expressions similar to Equation (3) for sea ice, a debris-covered glacier, freshwater lake ice and the West Greenland ice sheet, respectively. In the DEB model, we use an iterative Newton–Raphson method according to:

$$T_s(n + 1) = T_s(n) - \frac{F(T_s(n))}{F'(T_s(n))}, \tag{3}$$

where $F'(T_s)$, the derivative of the total surface flux with respect to T_s, is calculated numerically by the central difference method. At each time-step in the model an initial guess of $T_s(n = 0)$ must be made: for the first time-step it is set equal to the air temperature, T_a, and thereafter it is set at the value of T_s calculated for the previous time-step.

Equation (3) is calculated repeatedly until the point where $|T_s(n + 1) − T_s(n)| < 0.01$.

Debris internal temperatures

Several workers, including Greuell and Konzelmann (1994), Koh and Jordan (1995) and Pellicciotti and others (2009), have investigated the influence of subsurface heat conduction into debris-free ice and snow. This flux can be significant when there is a nonzero gradient of temperature with depth, or when some solar shortwave flux penetrates into the snow/ice. The conduction can be calculated from a heat-conservation equation based on Fourier's law, taking into account the partial derivatives of temperature, $T_{i,s}$, with respect to time, t, and depth, z:

$$\rho_{i,s} c_{i,s} \frac{\partial T_{i,s}}{\partial t} = \frac{\partial}{\partial z}\left(k_{i,s} \frac{\partial T_{i,s}}{\partial z}\right) + \frac{\partial Q}{\partial z} \qquad (4)$$

where $\rho_{i,s}$, $c_{i,s}$ and $k_{i,s}$ are, respectively, the density, specific heat capacity and thermal conductivity of the ice or snow. For the DEB model, we adapt Equation (4) to apply to a debris layer. The first term on the right-hand side represents heat conduction, while the second term generally accounts for radiative fluxes, Q, penetrating into an ice or snow layer from above. We can assume that no radiative fluxes penetrate rock, and therefore the second term, $\partial Q/\partial z$, can be ignored. The equation is then solved by dividing the debris layer into several calculation layers and applying a numerical algorithm with boundary conditions defined by the surface temperature, T_s, and the temperature of the debris base, which is in contact with the glacier ice and is assumed to remain at the melting point of ice, $T_f = 273.15$ K, during the ablation season, as justified by measurements. Generally the number of calculation layers, N, is chosen so the model calculates temperatures at 1 cm intervals, unless the cover is thinner than 5 cm, in which case the number of layers is fixed at 5. This method is fully described in the Appendix, and shows that despite a laborious proof the final algorithm can be applied with only a few lines of code, and is not computationally intensive.

Surface heat fluxes

Brock and others (2010) present equations for the heat fluxes on the surface of Miage glacier that are well justified by reference to existing parameterizations, and assessed for their suitability for a debris-covered surface. In this paper, the same equations are used, with some modifications. We apply the convention that positive fluxes are directed towards the debris surface, and all fluxes are in units of W m^{-2}. Table 1 displays all the main quantities used in the model, including 'constants', which should not change significantly across different sites, and 'parameters', which may vary across different sites.

Solar shortwave radiation

Incoming ($S\downarrow$) and reflected ($S\uparrow$) solar shortwave radiation data were used to compute net shortwave $S = S\downarrow − \uparrow$ at the debris surface. Alternatively, one can use $S = (1 − \alpha_d)S\downarrow$, where α_d is the debris albedo. For future applications in which the shortwave radiation has not been measured, the model could accept inputs from other models that calculate top-of-atmosphere shortwave and incorporate attenuation, diffusion, reflection and shadowing to give a value for the surface shortwave.

Longwave radiation

Downwelling longwave radiation, $L\downarrow$, is also supplied to the DEB model from data, but as with shortwave radiation it could be simulated in future applications. Upwelling longwave radiation is calculated from the Stefan–Boltzmann law:

$$L\uparrow = −\epsilon_d \sigma T_s^4, \qquad (5)$$

where ϵ_d is the debris surface emissivity and σ is the Stefan–Boltzmann constant.

Turbulent heat fluxes

The bulk aerodynamic method was used to calculate turbulent fluxes of sensible and latent heat. First, the stability of the surface layer is assessed by calculating the bulk Richardson number:

$$R_b = \frac{g(T_a − T_s)(z_a − z_{0m})}{T_m u^2}, \qquad (6)$$

where g is gravitational acceleration, z_a is the height of measurement of air temperature, z_{0m} is the surface roughness length for momentum and T_m is the mean air temperature between the surface and height z_a, calculated as $T_m = (T_a + T_s)/2$. R_b is used to calculate non-dimensional stability functions for momentum (Φ_m) heat (Φ_h) and moisture (Φ_v). For a stable surface layer, $R_b \geq 0$:

$$(\Phi_m \Phi_h)^{-1} = (\Phi_m \Phi_v)^{-1} = (1 − 5R_b)^2. \qquad (7)$$

For an unstable surface layer, $R_b < 0$:

$$(\Phi_m \Phi_h)^{-1} = (\Phi_m \Phi_v)^{-1} = (1 − 16R_b)^{0.75}. \qquad (8)$$

Now, sensible (H) and latent (LE) heat are calculated as

$$H = \rho_a \frac{c_a k_{vk}^2 u (T_a − T_s)}{\left(\ln\frac{z_a}{z_{0m}}\right)\left(\ln\frac{z_a}{z_{0t}}\right)} (\Phi_m \Phi_h)^{-1}, \qquad (9)$$

$$LE = \rho_a \frac{L_v k_{vk}^2 u (q_a − q_s)}{\left(\ln\frac{z_a}{z_{0m}}\right)\left(\ln\frac{z_a}{z_{0q}}\right)} (\Phi_m \Phi_v)^{-1}, \qquad (10)$$

where k_{vk} is von Kármán's constant, L_v is the latent heat of vaporization of water, q_a and q_s are specific humidities at the measurement height, z_a, and at the surface, respectively, calculated from relative humidity and temperature data by standard empirical formulae, and z_{0t} and z_{0q} are the surface roughness lengths for heat and humidity, respectively, considered equal to z_{0m}. The specific heat capacity of air, c_a, is corrected for a humid atmosphere using the formula $c_a = c_{ad}(1 + 0.84q)$, where c_{ad} is the specific heat capacity of dry air. The density of air, ρ_a, is calculated according to the ideal gas law:

$$\rho_a = \frac{p_a M_a}{R T_a}, \qquad (11)$$

where R is the universal gas constant and M_a is the molar mass of dry air. The air pressure, p_a, is estimated based on the altitude, H, of the glacier site:

$$p_a = p_{ssl}\left(1 − \frac{L_T H}{T_{ssl}}\right)^{\frac{g M_a}{R L_T}}, \qquad (12)$$

where p_{ssl} and T_{ssl} are the standard pressure and temperature at sea level, and L_T is the temperature lapse rate with altitude. We make the intuitive assumption that there can only be a latent heat flux at the debris surface when the surface is saturated (RH$_s$ is 100%), implying that there is either surface water to evaporate, or sufficient water vapour

Table 1. 'Constants' used in the DEB model, which are well known and should not change significantly across different sites, and 'parameters', which may vary across different sites. Default parameter values are given for Miage glacier and Villarrica. All parameter values are based on values given by Brock and others (2007, 2010), unless otherwise stated in the text

Constant	Symbol	Value	Unit
Gravitational acceleration	g	9.81	$m\,s^{-2}$
Von Kármán's constant	k_{vk}	0.41	
Stefan–Boltzmann constant	σ	5.67×10^{-8}	$W\,m^{-2}\,K^{-4}$
Universal gas constant	R	8.31	$J\,K^{-1}\,mol^{-1}$
Molar mass of dry air	M_a	0.02896	$kg\,mol^{-1}$
Standard sea-level pressure	p_0	101 325	Pa
Standard sea-level temperature	T_0	288.15	K
Air-temperature vertical lapse rate	L_T	0.0065	$K\,m^{-1}$
Latent heat of vaporization of water	L_v	2.476×10^6	$J\,kg^{-1}$
Latent heat of fusion of water	L_f	3.34×10^5	$J\,kg^{-1}$
Density of water	ρ_w	999.7	$kg\,m^{-3}$
Specific heat capacity of water	c_w	4181.3	$J\,kg^{-1}\,K^{-1}$
Specific heat capacity of dry air	c_{ad}	1005	$J\,kg^{-1}\,K^{-1}$
Density of ice	ρ_i	915	$kg\,m^{-3}$

Parameter	Symbol	Value (Miage)	Value (Villarrica)	Unit
Model time-step	Δt	3600	1800	s
Altitude of measurement site	H	2030	1900	m
Air temperature, wind and RH measurement height	z_a	2.16	2.00	m
Debris surface roughness length for momentum	z_{0m}	0.016	0.001	m
Debris layer thickness	d	0.23	various	m
Number of calculation layers	N	23	various	
Debris thermal conductivity	k_d	0.94	0.35	$W\,m^{-1}\,K^{-1}$
Debris density	ρ_d	1496	250	$kg\,m^{-3}$
Debris specific heat capacity	c_d	948	804	$J\,kg^{-1}\,K^{-1}$
Debris volumetric heat capacity	$C_d\,(=\rho_d c_d)$	1 418 208	201 000	$J\,m^{-3}\,K^{-1}$
Debris emissivity	ϵ_d	0.94	1	
Debris albedo	α_d	0.13	0.05	
Ice surface roughness length for momentum	z_{0i}	0.001	0.001	m
Ice emissivity	ϵ_i	0.97	0.97	
Ice albedo	α_i	0.34	0.50	

to condense. This condition is imposed by setting $LE = 0$ whenever $RH_s < 100\%$.

Heat flux due to precipitation

The heat flux due to precipitation is calculated in a similar manner to Hay and Fitzharris (1988) and A. Bliss (http://escholarship.org/uc/item/8r38754s):

$$P = \rho_w c_w w (T_r - T_s), \tag{13}$$

where ρ_w is the density of water, c_w is the specific heat capacity of water, w is the rainfall rate in $m\,s^{-1}$ and T_r is the rain temperature, which in the absence of complete information is set equal to the measured air temperature, T_a. P is often ignored in glacier studies because it tends to be extremely small, but for future studies of glacier retreat under shifting global precipitation regimes it could be an important heat flux, for example on Himalayan glaciers that experience monsoon rains. For this paper, precipitation data are not available for the exact glacier sites, but we make use of data from the nearby Lex Blanche station. The effects of precipitation could be more accurately modelled using rain-gauge and lysimeter data to calculate how much rain evaporates from the debris, and how much percolates through the debris layer to supply a heat flux to the ice (Sakai and others, 2004). This could potentially improve the accuracy of the DEB model's latent heat, precipitation heat

flux and internal temperature calculations. However, given the absence of the necessary data, this is left as a project for future work. Our approach considers only the effect of precipitation heat flux at the top of the debris layer, where the surface energy balance (Equation (1)) is defined.

Conductive heat flux

The conductive heat flux, G, at the debris surface is calculated based on the temperature gradient at the top of the debris layer, approximated using the surface temperature, T_s, and the temperature, $T_d(1)$, at the first calculation layer for debris:

$$G = k_d \left(\frac{dT_d}{dz}\right)_{surface} \approx k_d \frac{T_d(1) - T_s}{h}, \tag{14}$$

where h is the thickness of each calculation layer (usually set to 1 cm) and k_d is the thermal conductivity of the debris.

Calculating glacier melt

The only heat flux considered to reach the glacier ice is a conductive flux, G_i, which depends on the temperature gradient at the base of the debris:

$$G_i(t) = -k_d \left(\frac{dT_d}{dz}\right)_{base} \approx k_d \frac{T_d(N-1) - T_f}{h}. \tag{15}$$

The ice melt (m w.e.) for the time-step, assuming no further

downward conduction of heat, can then be calculated as:

$$M = \frac{G_i \Delta t}{\rho_i L_f},$$ (16)

where Δt is the model time-step, ρ_i is the density of ice and L_f is the latent heat of fusion of water. A caveat is built in, so that, if the melt rate is calculated to be negative (due to negative temperatures in the debris layer above), it is set to zero; thus, the DEB model implicitly assumes there is no accumulation in the ablation zone because all meltwater runs off immediately without pooling and refreezing.

Overall model structure

The run structure of the DEB model is dominated by the Newton–Raphson iteration procedure for solving surface temperature. It is summarized in Figure 2.

Bare-ice model

To quantify the effects of debris on ablation, a bare-ice melt model was developed for comparison with the DEB model. It includes the assumptions that the ice surface remains at $T_s = 0°C$ and can be considered saturated for the purposes of latent heat calculations. Melt rate (m w.e.) for the time-step is calculated from the total sum of heat fluxes:

$$M = \frac{\Delta t}{\rho_i L_f} [(1 - \alpha_i) S\downarrow + L\downarrow + L\uparrow + H + LE + P],$$ (17)

where α_i is the ice albedo, and all the heat fluxes are calculated using the same equations described above, but with emissivity and surface roughness lengths corrected for ice instead of debris (see Table 1). The downwards conductive flux, G, is considered negligible.

RESULTS AND DISCUSSION

Unless otherwise stated, the r^2 values presented in this section represent the Nash–Sutcliffe model efficiency coefficient, and refer to the fit between modelled and measured surface temperature, T_s.

Fully mechanistic model

The DEB model can be considered mechanistic at this stage, since all the processes and quantities involved are informed by empirical equations and field measurements as far as possible; none have been adjusted to fit a dataset. Also, all the variables were measured at one site and have not been extrapolated to other areas. As can be seen in Figure 3a, the default parameter values in Table 1 are sufficient for the model to produce surface temperature values with a very good fit ($r^2 = 0.9437$) to the data across the whole 2005 ablation season. Similar fits were acquired for 2006 ($r^2 = 0.9469$) and 2007 ($r^2 = 0.9421$).

Figure 4a shows the mean daily cycle of modelled debris temperatures across the 2005 ablation season. There is an obvious lag with depth, so the maximum temperature at the bottom of the layer occurs ~3–4 hours after the maximum surface temperature. This is to be expected since heat conduction through the debris will take some time, and it concurs with Nicholson and Benn (2006), who reported lags of 3–4 hours between the surface temperature and 20 cm depth in a debris layer on Ngozumpa Glacier, Nepal. Figure 4b illustrates this lag in more detail: there are nonlinear temperature profiles when the layer is warming or
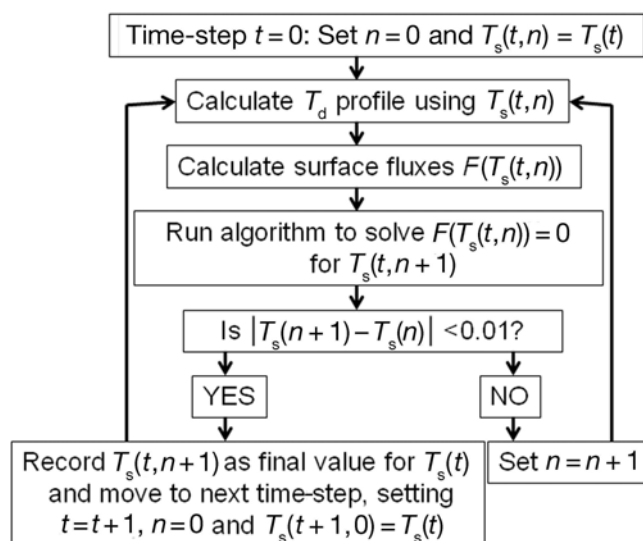

Fig. 2. Flow chart illustrating the DEB model run progression, centred around the Newton–Raphson algorithm for calculating surface temperature.

cooling, but approximately linear profiles at the warmest (1500 h) and coldest (0600 h) times of day.

However, a discrepancy arises when the modelled temperature is compared to data. Figure 3b shows the modelled debris temperature at 15 cm depth alongside measured data for the same depth, which were collected using thermistors at a separate site near the AWS between 0100 h on 21 June and 1900 h on 24 July. The modelled mean (4.4°C) and measured mean (4.1°C) temperatures are very similar, but the overall fit is poor ($r^2 = 0.5173$) because the modelled temperature lags behind the data by ~3 hours. This lag is not a function of the model's numerical procedures and finite time-step, since the lag remains the same even when data are interpolated to run the model with a much shorter (1 min) time-step. The lag may arise due to varying debris properties that affect thermal diffusivity at the two sites, such as the prevalence and connectivity of void spaces which could affect non-conductive processes such as windpumping (Humlum, 1997). Alternatively, there may be an error in the measured 15 cm temperature due to direct solar heating of the thermistor cables that were lying on the debris surface: conduction down the cables could cause temperatures to rise too quickly in the morning. These are areas that should be investigated using more accurate measurements of the debris thermal profile. In the meantime, any lag-induced error in temperature gradient at the debris base, which determines melt, will be very small and should even out over time, meaning that the main quantities of interest (mean daily or seasonal melt rates) should be unaffected. Figure 3c displays the modelled hourly melt rate in mm w.e. h^{-1} and, as might be expected, the melt rate follows a similar trend to surface temperature (Fig. 3a). The calculated mean daily melt rates, M_{day}, were 14.5, 15.4 and 13.7 mm w.e. d^{-1} over the ablation seasons of 2005, 2006 and 2007, respectively. Figure 3d shows mean daily cycles of temperature and surface heat fluxes for 2005, 2006 and 2007, and Table 2 presents the mean, maximum and minimum of these cycles. In all three years the mean modelled surface temperatures are higher than the data by just over 1°C. There are many reasons why this could occur, but one physical interpretation is that
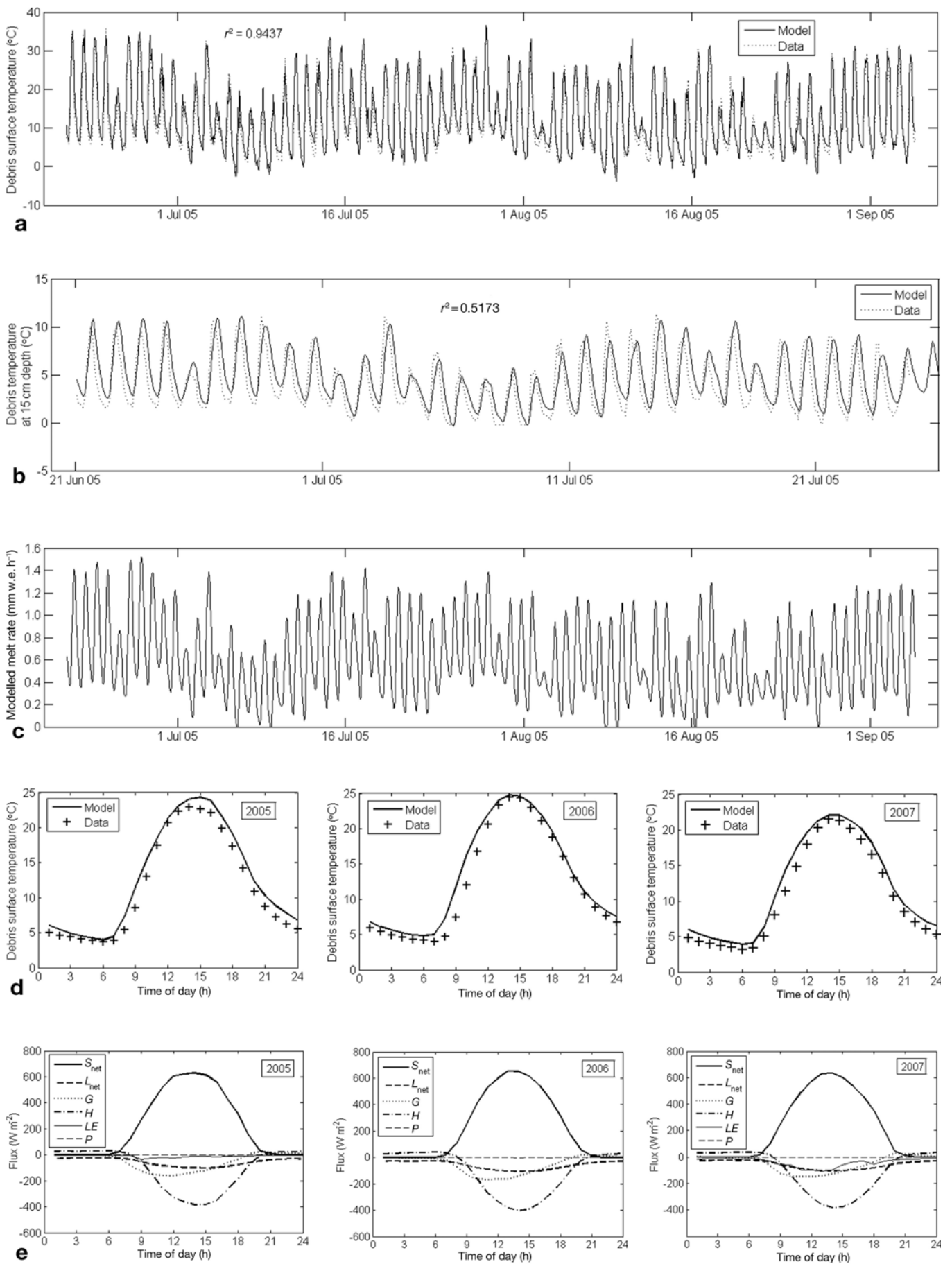
Fig. 3. Model outputs for the Miage glacier AWS site (2030 m a.s.l.) using the default parameter values listed in Table 1. (a) Modelled and measured debris surface temperature, (b) debris internal temperature at 15 cm depth and (c) modelled hourly melt rate for the 2005 ablation season. (d, e) Mean daily cycles of modelled and measured debris surface temperature (d) and surface heat fluxes (e), for the ablation seasons of 2005, 2006 and 2007.
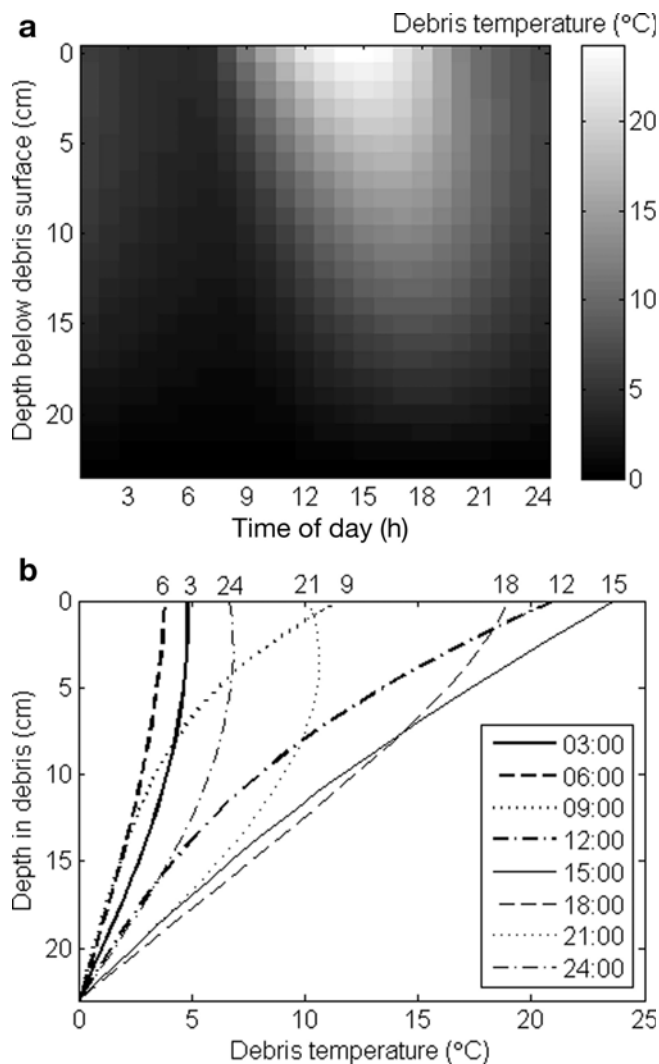
Table 2. Mean, daily maximum and daily minimum debris surface temperatures on Miage glacier (°C) as measured (data) and as calculated by the DEB model, for 2005, 2006 and 2007

Year	Mean	Maximum	Minimum
2005 (data)	11.5	22.9	3.7
2005 (model)	12.7	24.3	4.0
2006 (data)	12.2	24.5	4.0
2006 (model)	13.3	24.8	4.8
2007 (data)	10.6	21.5	3.2
2007 (model)	11.9	22.1	3.9

Fig. 4. Modelled debris temperature during the ablation season on Miage glacier in 2005. (a) Average value for every hour of the day and (b) line plots for selected times of day.

the data were calculated from radiative measurements of upwelling longwave; this required a value for surface emissivity, which may have been overestimated.

Figure 3e shows the mean daily cycles of surface heat fluxes. The mean latent heat flux (LE) values were calculated for 2005 and 2007 using only those data points where surface RH data were available, and there is no latent heat flux for 2006 due to lack of data. The wettest year was 2007, with considerable evaporation, as reflected in the relatively large negative latent heat flux and lower surface temperature.

Sensitivity analysis

Arguably, the parameters with greatest uncertainty in the model are the physical properties of the debris layer: ϵ_d, z_{0m}, k_d, ρ_d and c_d. In particular, the model in its current form makes the assumption that k_d, ρ_d and c_d are constant with depth, which is undoubtedly not the case in the real world. Debris layers tend to have an inhomogeneous structure, with dry rubble and boulders on top containing considerable air spaces, and smaller rubble and fine particles beneath, which may often be saturated with water near the glacier ice. A more advanced model could account for this variation by allowing physical properties to vary with depth; however, a verification of the model would require detailed data on

internal debris temperature and water content, and is beyond the scope of this paper. Instead, the parameters are investigated via a standard sensitivity analysis. Table 3 illustrates how the model's r^2 fit to surface temperature, and the mean daily melt rate, M_{day}, on Miage glacier in 2005 respond to changes in the debris properties. Each parameter is varied from its default value by ±10%, except for ϵ_d, because it does not make physical sense to increase it above 1. Also, because ρ_d and c_d are always multiplied together in the model, they are considered as one parameter, $C_d = \rho_d c_d$, the volumetric heat capacity. It should be noted that this analysis is very specific to the 2005 season on Miage glacier; and given that the parameters almost certainly influence each other in ways that are difficult to quantify, it would not make physical sense to change any one parameter dramatically without changing the others. Therefore the changes in each parameter are kept relatively low (up to 10%). This reflects our aim to be entirely mechanistic wherever possible; the analysis is more a tool for deciding which parameters are important and could therefore benefit from more accurate estimates in the field.

The model fit and melt rate are relatively insensitive to C_d and z_{0m}. The fit improves slightly upon increasing ϵ_d, accompanied by a small decrease in melt rate due to greater longwave emission from the surface. A ±10% change in k_d produces up to a 10% change in melt rate. This highlights the importance of k_d in the debris energy balance. However, although the average k_d for a debris layer can be estimated by observing melt rates (Brock and others, 2010), it is hard to quantify how it may vary with depth; solid rock tends to have k_d values ~2–7 W m^{-1} K^{-1}, while the air spaces in between have a much lower k_d, ~0.025 W m^{-1} K^{-1}. The heat transfer in the upper debris may be dominated more by turbulent processes than conduction, and water at the base of the debris, with thermal conductivity ~0.58 W m^{-1} K^{-1},

Table 3. Response of r^2 and M_{day} upon changing parameter values, for the 2005 ablation season on Miage glacier

Parameter	Change	r^2	M_{day}
			mm w.e.
k_d	±10%	−0.56 to +0.47%	−9.9 to +8.1%
C_d	±10%	−0.06 to +0.002%	−0.55 to +0.50%
ϵ_d	±5%	−2.2 to +0.77%	+4.5 to −5.2%
z_{0m}	±10%	−0.28 to +0.20%	+0.49 to −0.44%

Table 4. Response of the DEB model's fit to surface temperature data, r^2, and mean daily melt rate, M_{day} (mm w.e.), when individual heat fluxes were set to zero. All are significant changes in fit to the 95% confidence level, except that marked with an asterisk. For latent heat flux, LE, the fit refers only to those times when surface RH was measured (1702 data points in 2005, 533 in 2007)

Year	Flux removed	Change in r^2	M_{day}
2005	None	n/a	14.5
2006	None	n/a	15.4
2007	None	n/a	13.7
2005	$S\downarrow$	−1.6451	5.8
2005	$S\uparrow$	−0.0277	15.1
2005	$L\downarrow$	−2.0423	2.1
2005	$L\uparrow$	−1.1154	23.1
2005	G	−0.9540	13.2
2005	H	−3.9322	25.9
2005	P	−0.0002	14.5
2006	P	−0.0001*	15.4
2007	P	−0.0002	13.7
2005	LE	−0.0106	13.7
2007	LE	−0.0490	13.7

will add further complicating effects. These phenomena should be a focus of future studies.

Significance of variables

The good fit to data provided when running the model with default parameter values provides a strong indication that all the physical theory implemented in the model is sound. However, it is useful for both model parsimony and scientific insight to test whether individual components of the model are entirely necessary for a strong fit. In this case, the components of most interest are the individual heat fluxes. The importance of each flux was assessed by removing the equations for calculating the flux (setting the flux to zero) and calculating the new fit of the model. Based on the results in Table 4, the shortwave, longwave, conductive and sensible heat flux equations are clearly essential for the model to perform well, because the model r^2 fit to surface temperature suffers significantly when any of them are removed. The results also suggest that latent heat, LE, produces a smaller, though still significant, improvement in fit for the periods in which it was calculated.

Table 5. Change in model fit, r^2, on setting each input variable in turn to its mean value for the whole ablation season. All are significant changes in fit to the 95% confidence level, except those marked with asterisks. RH_s was not measured in 2006

Variable	2005	2006	2007
$S\downarrow$	−0.7154	−0.6842	−0.7782
$S\uparrow$	−0.0194	−0.0126	−0.0223
$L\downarrow$	−0.0090	−0.0079	−0.0042
T_a	−0.1258	−0.1774	−0.1558
u	−0.0119	−0.0105	−0.0208
RH_a	+0.0027	+0.000007*	+0.0009
w	−0.00005*	+0.00004*	+0.0002
RH_s	−0.0106	n/a	−0.0491

Table 6. Model fit to surface temperature data when the only variability in the model comes from solar shortwave radiation and air-temperature data.

	Year		
	2005	2006	2007
r^2	0.9141	0.9280	0.9032

The change in r^2 on removing the heat flux from precipitation, P, from the model is tiny. Even so, it is deemed significant in 2005 and 2007, but not 2006 (assessed by performing statistical F-tests on the 'improvement' in fit incurred by including the flux). This suggests that P may have a significant effect on the glacier surface energy balance. However, such results should be treated with caution; it is difficult to define the degrees of freedom in a nonlinear model which uses each variable multiple times and has no parameters adjusted to fit, and the F-test will tend to place undue significance on even tiny improvements in fit for such a large dataset. There is also a considerable unquantifiable error caused by using precipitation data from Lex Blanche, 4 km from the glacier. For these reasons, and given that the model provides a very significant fit without P, precipitation data are deemed unnecessary for applying our model to debris-covered alpine glaciers in its current form, but it is certainly an area for further study. The heat flux from precipitation could become more significant in areas of heavy rainfall, such as monsoon regimes in the Himalaya, and build-up of rainwater within debris could have strong effects on heat conduction. Therefore precipitation measurements could form a valuable part of future fieldwork on debris-covered glaciers. Similar F-tests were used to assess whether the variability in each input variable was essential for a good fit to surface temperature, for purposes of simplifying the model. Table 5 presents the change in model fit when each variable was set to its mean value for the whole ablation season, thus removing its variability – an approach inspired by the 'model reduction' techniques described by Cox and others (2006) and Crout and others (2009). This shows that w, the precipitation data from Lex Blanche, either gives no significant improvement in fit, or actually makes the fit worse (r^2 increases when it is removed, implying that the precipitation data add unnecessary noise to the model). More interestingly, the same can be said about RH_a, the relative humidity in air measurements made at the Miage study site. This implies that the improved fit provided by adding the heat flux from precipitation, P, and latent heat, LE, to the model, as reported above, arises solely from the other variables and parameters included in the equations.

Table 5 also shows that the improvements in fit on including variability in upwelling shortwave radiation, $S\uparrow$, downwelling longwave radiation, $L\downarrow$, wind speed, u, and surface relative humidity, RH_s, are very small. These results indicate that the melt rates of debris-covered glaciers in the Alps could be modelled to a reasonable degree of accuracy using only shortwave radiation and air-temperature data, as has been noted for clean glaciers in the Alps (Pellicciotti and others, 2005). This was tested by setting all variables except $S\downarrow$ and T_a to their mean values for the ablation season, and Table 6 shows that the model still provides a strong fit to
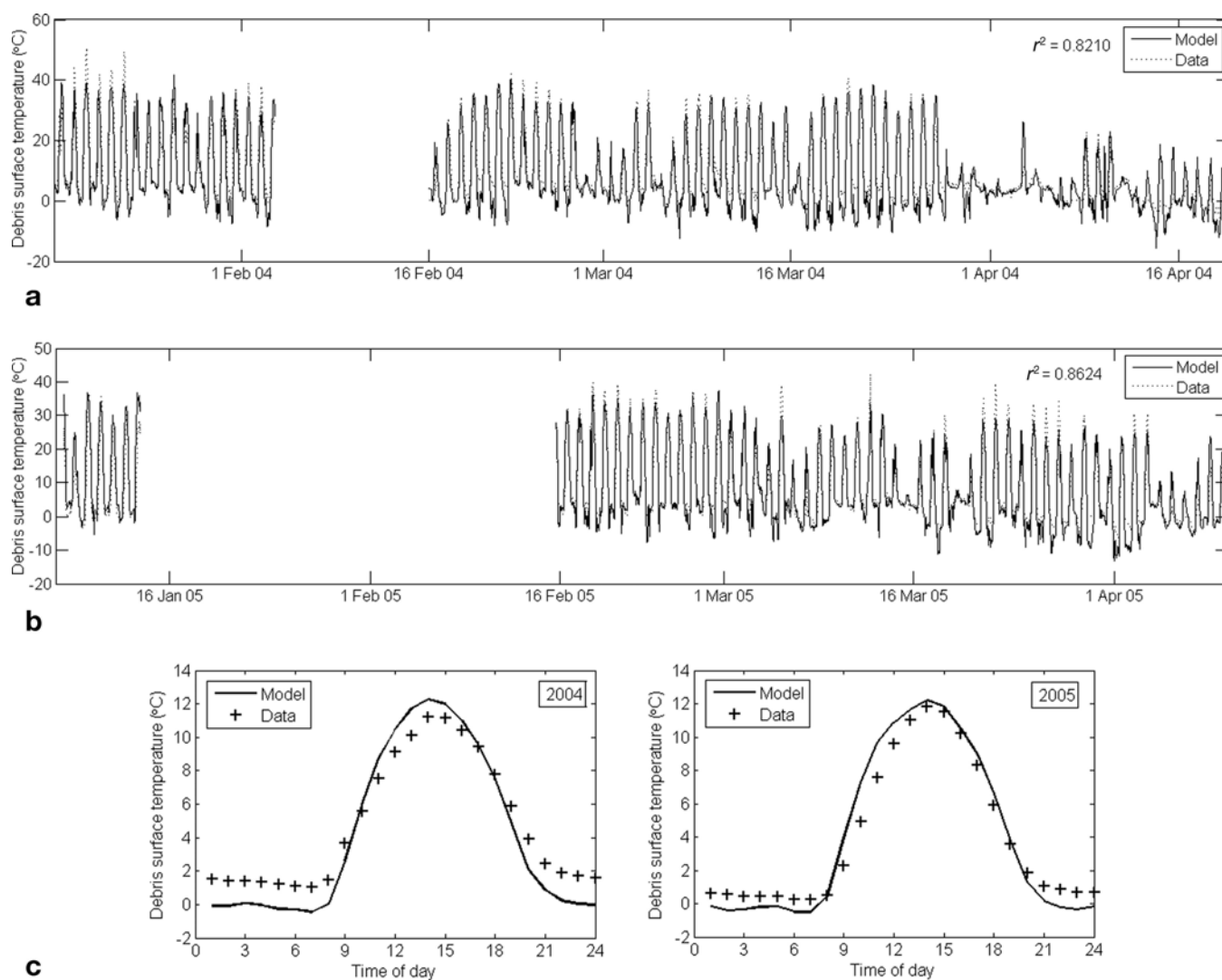
Fig. 5. Model outputs for Villarrica glacier using the default parameter values listed in Table 1. Modelled and measured debris surface temperature in (a) 2004 and (b) 2005, and mean daily cycles of surface temperature in (c) 2004 and (d) 2005.

surface temperature data ($r^2 > 0.9$) for all three years. This is encouraging for developing simpler models of melt rates on such glaciers. However, more work is required to determine whether the same simplifying assumptions could be made for glaciers in other mountain ranges. In any case, the debris layer thickness and thermal properties have a huge effect on melt rates and should be included in any model if it is to be generalized to areas where these properties are different. Remote-sensing approaches to mapping debris thickness (e.g. Mihalcea and others, 2008) could provide the necessary inputs to such models.

It should be noted that the removal of RH$_s$ variability from the model amounts to completely removing the latent heat flux, LE, due to the way the model is formulated. This results in a moderate but significant reduction in r^2, implying that the variability in RH$_s$ improves the model. An accurate calculation of latent heat flux by bulk-transfer theory will always require data on surface humidity, but RH$_s$ is generally not measured on or near glacier sites, or predicted by global or regional-scale climate models. We conclude that although latent heat flux is of secondary importance for useful energy-balance models of alpine glaciers, supporting the findings of Lang (1981) for clean glaciers, there remains a challenge for future field and modelling studies to

parameterize it without such requirements on surface data, especially for other areas of the world, where latent heat fluxes may become more significant.

Cross-validation

To determine whether the DEB model could be generalized to other glacier systems, it was tested using data collected on the tephra-covered glacier of Villarrica volcano in 2004 and 2005 (described by Brock and others, 2007). Data were collected half-hourly according to a regime similar to that on Miage glacier, but given a lack of surface RH and precipitation data it was not possible to calculate latent heat flux, LE, or the flux from precipitation, P. Furthermore, given the uneven spread of tephra compared to the debris cover on Miage glacier, the surface temperatures were not measured directly beside the AWS, but on tephra banks up to 100 m away. These sites had tephra thicknesses of $d = 0.32$ m in 2004 and $d = 0.13$ m in 2005. It should also be noted that the surface temperature was measured using thermistors which experience greater errors than the radiative temperature measurements used at Miage glacier, due to occasional exposure to direct solar heating or wind cooling. The default parameter values for Villarrica are shown in Table 1. Figure 5 shows the surface temperatures calculated using the DEB
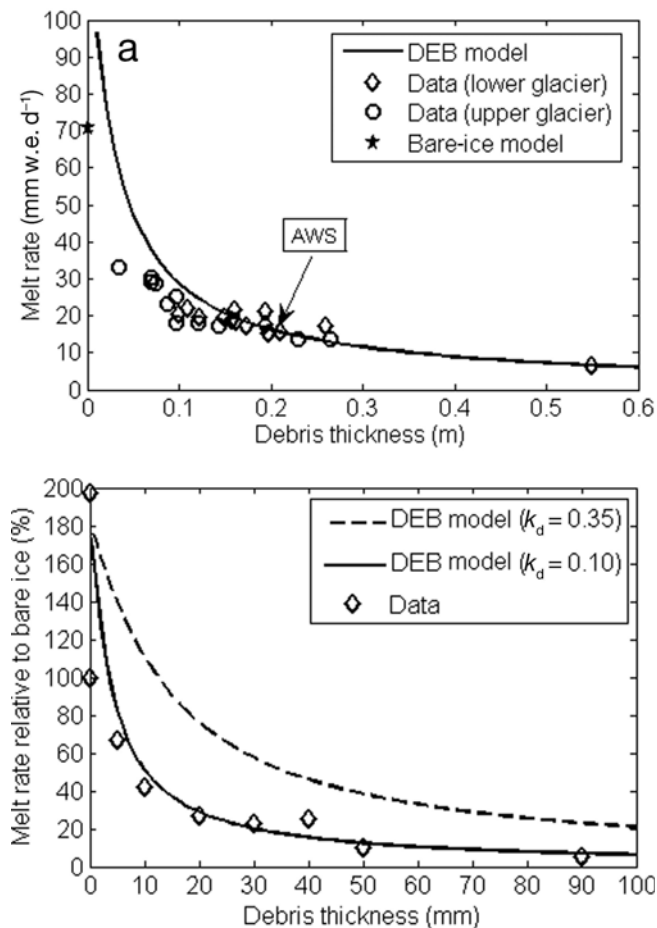
Fig. 6. Modelled and observed mean daily melt rates plotted against debris thickness, for (a) Miage glacier and (b) Villarrica glacier. Note that the data used to run the DEB model for Miage glacier (a) were recorded at an AWS (indicated data point) on the lower glacier. Melt data from the upper glacier, where meteorological conditions are quite different, are shown separately because they should not be directly compared to the curve.

model for 2004 and 2005, which provide a good fit to data in both years, especially considering that the input data were measured at a different site to the surface temperature. However, as Figure 5c and d show, the model consistently underestimated night-time surface temperatures by as much as 2°C. This can be explained by noting that air temperature on Villarrica dropped below 0°C on several occasions during measurement. This means that the assumption in the DEB model, that the debris/ice interface remains at 0°C, may not be suitable; in fact the interface temperature probably goes below 0°C. The DEB model compensates for this incorrect assumption by setting T_s lower than it should be. Similar problems were found by Nicholson and Benn (2006) for melt models at Larsbreen, Svalbard; they argue that these colder regions may require models to include conductive heat fluxes into the ice. Further work is required to make the DEB model capable of calculating accurate debris temperatures for this situation, given that some energy is required to heat up the ice and debris before melting can take place again.

Effects of debris thickness

Perhaps the most interesting and useful application of the DEB model is that it can be used to estimate mean daily melt rates as a function of debris thickness. The curve in Figure 6a shows the results of several model runs for Miage glacier in 2005 using varying values of debris thickness, d, plotted with data collected at several sites on the glacier. No goodness of fit is calculated for Figure 6a because, although the model is run with meteorological inputs from the AWS site, the data points represent sites at a variety of other positions on the glacier, where variations in altitude, aspect and shadowing result in very different meteorological conditions. In particular, data from the upper glacier (where the glacier turns north, elevation increases more sharply and the glacier experiences greater shadowing effects from the Mont Blanc massif) are shown with different markers to indicate that they should not be directly compared to the model curve. Despite this limitation, the DEB model matches the data well, not only at the AWS site (indicated) but also at higher debris thicknesses up to 55 cm. However, it overestimates the melt rate for debris layers thinner than ~14 cm. This is partly because most of the thin-debris measurements were taken at higher parts of the glacier, but may be further explained by an observed positive relationship between k_d and d (Brock and others, 2010). The bare-ice model predicts a higher melt rate than was measured (71 vs 58 mm w.e. d^{-1}), but again it should be noted that the bare-ice measurements were made some distance up-glacier from the AWS. Furthermore, the colder surfaces presented by thinner debris layers and bare ice during the ablation season are likely to reduce air temperatures relative to a 23 cm layer, and the atmospheric boundary layer may have a very different structure, with the surface becoming a sink for sensible heat rather than a source. Such discrepancies could be partly taken into account in distributed models by applying suitable lapse rates, dependent on altitude and debris patterns.

Figure 6b shows similar predictions for Villarrica glacier, using a 6 day block of meteorological data from January 2005. The model predictions are plotted with data recorded around the same time during an experiment in which ablation was measured on artificial plots with various debris thicknesses. The sub-debris melt rates are shown relative to bare-ice melt rates to account for differences between the experiment site and the AWS site. As can be seen, the melt rate is very sensitive to thermal conductivity; with the default value of $k_d = 0.35$, the model overestimates the melt rate, while using a value of $k_d = 0.10$ provides a good match to the data. This may be because the default value of 0.35 was calculated from measurements in 2004 on thicker, natural debris layers (11–32 cm); these were subjected to compression under a winter snowpack, and may even have been re-exposed after previous incorporation inside the glacier ice. Conversely, the artificial tephra covers created to collect the data in Figure 6b had looser, lighter structures with more air pockets, meaning they would undoubtedly show lower thermal conductivity than the compact layer. In any case, this result highlights the importance of debris thermal conductivity as a parameter to consider in any study of a debris-covered glacier. Interestingly, the DEB model predicts that very thin debris layers will produce a melt rate higher than the bare-ice melt rate. This enhancement was not seen in the Miage glacier melt data, but a large melt enhancement, of 197%, was observed for a very thin dusting of tephra (estimated by Brock and others, 2007, to have thickness 0.25 mm) on one of the Villarrica experimental plots (the upper data point close to the y-axis in Figure 6b). This finding can be related to a well-established feature of

debris-covered glaciers, the 'Østrem curve' (Østrem 1959), which shows that very thin debris covers increase ablation rates by darkening the surface, while debris covers thicker than a certain 'critical thickness' reduce ablation. The critical thickness has been shown to vary considerably across glaciers in different locations and with different types of debris cover (Kirkbride and Dugmore, 2003). As Figure 6 shows, the melt rate certainly increases for thin debris layers, but there is no sign that it reaches a maximum and then decreases towards the bare-ice melt rate as the debris thickness tends towards zero. In reality, a smooth Østrem curve may arise for reasons that are not incorporated in the DEB model. For example, the transfer of heat is not restricted to the vertical dimension, and the melt rate at one point will be affected by its immediate surroundings. In particular, one can observe that thin debris layers tend to be more sparsely scattered than thicker layers, exposing more high-albedo areas of ice that may reduce the melt rate. For debris layers made of dust or small particles, the situation may be more complicated, as shown by Adhikary and others (2002), who demonstrated that a uniform dust layer on snow begins to aggregate as the snow melts, thus reducing the ablation rate. On Miage glacier, where the scattered debris cover may vary from sand-sized particles to huge boulders, the situation can be approximated by defining a 'patchiness' parameter, r_{id}, representing the ratio of exposed ice to debris-covered ice. The melt rate can then be calculated as:

$$M = r_{id}M_{bare} + (1 - r_{id})M_{debris}, \qquad (18)$$

where M_{bare} is the melt rate for bare ice, and M_{debris} is the melt rate under a debris layer. r_{id} was defined by an exponential decay dependence on the debris thickness, d, simulating the fact that as the debris layer thickens, less ice will be exposed:

$$r_{id} = e^{-Cd}, \qquad (19)$$

where C is a constant. Figure 7 shows the melt rates calculated in this manner for Miage glacier in 2005, with $C = 20$ (note that this value is not based on observations, and is chosen arbitrarily for the purposes of our 'thought experiment'). The top curve uses the bare-ice melt rate calculated by our model ($= 71\,mm\,w.e.\,d^{-1}$), and the other two use bare-ice melt rates of 50 and $30\,mm\,w.e.\,d^{-1}$, to show that the effect is enhanced when the thin-debris melt rate is significantly higher than the bare-ice melt rate. The lines closely resemble Østrem curves. This suggests an interesting proposition for future field studies: quantifying r_{id} for various types and thicknesses of debris layers, and thus how it affects glacier melt rates

SUMMARY AND CONCLUSIONS

We have presented the DEB model, a detailed energy-balance model for a debris-covered glacier, which centres around an iterative calculation of surface temperature and includes conduction through the debris layer. The fact that this approach accurately reproduces long-term, high-resolution surface temperature data on two very different debris-covered glaciers, without fitting any parameters, is a satisfying indication that the assumptions and physics used to calculate surface heat fluxes are accurate, and the model is generalizable to different systems. The DEB model and the extensive dataset from Miage glacier allow a thorough statistical analysis of different aspects of energy balance at a
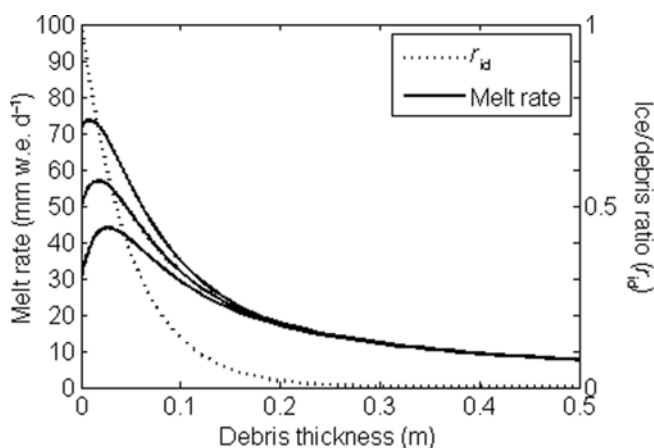

Fig. 7. Melt rates (solid curves) over a scattered debris cover, calculated using the DEB model and a bare-ice model with Miage glacier data. The ratio of exposed ice to debris-covered ice, r_{id}, is represented by the dotted curve (note that this curve is not based on any observed data, and is chosen arbitrarily for the purposes of this theoretical exercise). The solid curves were calculated by assuming bare-ice melt rates of, from top to bottom, 71 (the bare-ice model prediction), 50 and $30\,mm\,w.e.\,d^{-1}$.

debris surface, which helps to justify some assumptions that have been made in previous energy-balance models; for example, it indicates that the heat flux from precipitation is negligible for alpine glaciers, and that latent heat can be omitted without large losses in model performance. The main advantage of the DEB model is that it calculates the ice melt rate beneath supraglacial debris directly from meteorological data, without the need for surface temperature measurements. Hence, it can be applied to most of the world's debris-covered glaciers, since meteorological data are likely to be available, even if these come from a re-analysis program. The main challenge, particularly in glacial modelling at a regional scale, is in acquiring information on the extent, thickness and thermal properties of supraglacial debris covers. Such data could be obtained via remote sensing (e.g. Paul and others, 2004; Mihalcea and others, 2008) combined with suitable field validation (e.g. Brock and others, 2010). The DEB model could also be used to assess future meltwater production from debris-covered glaciers using climate-model outputs, but such an approach would require understanding of potential changes in supraglacial thickness and extent over time; processes which are currently poorly understood. The DEB model is a very detailed approach to glacier-melt prediction, and is probably more complicated than a melt model needs to be for most practical applications (e.g. as a component in large-scale hydrological catchment models). As has been shown, not all the simulated processes are essential for good model performance in both the Alps and the Andes, since model efficiency is dominated by just two input variables: air temperature and incoming shortwave radiation. It would be useful to develop a family of simpler, empirical models based around the same variables as the DEB model, and compare them on a thorough statistical basis using model-selection criteria (e.g. Cox and others, 2006). In the interests of pure science and understanding of glacier thermodynamics, the DEB model presents a useful platform for investigating even more detailed processes within a debris-covered glacier (e.g. variations in structure, moisture, and

hence thermal properties, with depth in the debris layer). For application to colder regions, the model should include downwards conduction into ice, which would decrease melt slightly at times when the ice acts as a heat sink (Pellicciotti and others, 2010). Finally, in the context of large-scale distributed models, the DEB model should be easy to combine with existing models for debris-free ice and snow, but may require more development if the distributed models were to include the effects of meltwater pooling and refreezing, or bare-ice slopes and cliffs that could present isolated areas of high melt rates (Sakai and others, 1998; Purdie and Fitzharris, 1999).

REFERENCES

Adhikary, S., Y. Yamaguchi and K. Ogawa. 2002. Estimation of snow ablation under a dust layer covering a wide range of albedo. *Hydrol. Process.*, **16**(14), 2853–2865.

Arnold, N.S., I.C. Willis, M.J. Sharp, K.S. Richards and W.J. Lawson. 1996. A distributed surface energy-balance model for a small valley glacier. I. Development and testing for Haut Glacier d'Arolla, Valais, Switzerland. *J. Glaciol.*, **42**(140), 77–89.

Bolch, T., M. Buchroithner, T. Pieczonka and A. Kunert. 2008. Planimetric and volumetric glacier changes in the Khumbu Himal, Nepal, since 1962 using Corona, Landsat TM and ASTER data. *J. Glaciol.*, **54**(187), 592–600.

Brock, B.W. and N.S. Arnold. 2000. A spreadsheet-based (Microsoft Excel) point surface energy balance model for glacier and snowmelt studies. *Earth Surf. Process. Landf.*, **25**(6), 649–658.

Brock, B., A. Rivera, G. Casassa, F. Bown and C. Acuña. 2007. The surface energy balance of an active ice-covered volcano: Villarrica Volcano, southern Chile. *Ann. Glaciol.*, **45**, 104–114.

Brock, B.W., C. Mihalcea, M.P. Kirkbride, G. Diolaiuti, M.E.J. Cutler and C. Smiraglia. 2010. Meteorology and surface energy fluxes in the 2005–2007 ablation seasons at the Miage debris-covered glacier, Mont Blanc Massif, Italian Alps. *J. Geophys. Res.*, **115**(D9), D09106. (10.1029/2009JD013224.)

Cox, G.M., J.M. Gibbons, A.T.A. Wood, J. Craigon, S.J. Ramsden and N.M.J. Crout. 2006. Towards the systematic simplification of mechanistic models. *Ecol. Model.*, **198**(1–2), 240–246.

Crout, N.M.J., D. Tarsitano and A.T. Wood. 2009. Is my model too complex? Evaluating model formulation using model reduction. *Environ. Model. Softw.*, **24**(1), 1–7.

Greuell, J.W. and T. Konzelmann. 1994. Numerical modeling of the energy balance and the englacial temperature of the Greenland ice sheet: calculations for the ETH-Camp location (West Greenland, 1155 m a.s.l.). *Global Planet. Change*, **9**(1–2), 91–114.

Hay, J.E. and B.B. Fitzharris. 1988. A comparison of the energy-balance and bulk-aerodynamic approaches for estimating glacier melt. *J. Glaciol.*, **34**(117), 145–153.

Humlum, O. 1997. Active layer thermal regime at three rock glaciers in Greenland. *Permafrost Periglac. Process.*, **8**(4), 383–408.

Kellerer-Pirklbauer, A. 2008. The supraglacial debris system at the Pasterze Glacier, Austria: spatial distribution, characteristics and transport of debris. *Z. Geomorphol. NF*, **52**, Suppl. 1, 3–25.

Kirkbride, M.P. 1993. The temporal significance of transitions from melting to calving termini at glaciers in the central Southern Alps of New Zealand. *Holocene*, **3**(3), 232–240.

Kirkbride, M.P. and A.J. Dugmore. 2003. Glaciological response to distal tephra fallout from the 1947 eruption of Hekla, south Iceland. *J. Glaciol.*, **49**(166), 420–428.

Klok, E.J. and J. Oerlemans. 2002. Model study of the spatial distribution of the energy and mass balance of Morteratsch-gletscher, Switzerland. *J. Glaciol.*, **48**(163), 505–518.

Koh, G. and R. Jordan. 1995. Sub-surface melting in a seasonal snow cover. *J. Glaciol.*, **41**(139), 474–482.

Lang, H. 1981. Is evaporation an important component in high Alpine hydrology? *Nord. Hydrol.*, **12**(4–5), 217–224.

Launiainen, J. and B. Cheng. 1998. Modelling of ice thermo-dynamics in natural water bodies. *Cold Reg. Sci. Technol.*, **27**(3), 153–178.

Mihalcea, C., C. Mayer, G. Diolaiuti, A. Lambrecht, C. Smiraglia and G. Tartari. 2006. Ice ablation and meteorological conditions on the debris-covered area of Baltoro Glacier, Karakoram, Pakistan. *Ann. Glaciol.*, **43**, 292–300.

Mihalcea, C. and 7 others. 2008. Using ASTER satellite and ground-based surface temperature measurements to derive supraglacial debris cover and thickness patterns on Miage Glacier (Mont Blanc Massif, Italy). *Cold Reg. Sci. Technol.*, **52**(3), 341–354.

Nakawo, M. and G.J. Young. 1981. Field experiments to determine the effect of a debris layer on ablation of glacier ice. *Ann. Glaciol.*, **2**, 85–91.

Nicholson, L. and D.I. Benn. 2006. Calculating ice melt beneath a debris layer using meteorological data. *J. Glaciol.*, **52**(178), 463–470.

Østrem, G. 1959. Ice melting under a thin layer of moraine, and the existence of ice cores in moraine ridges. *Geogr. Ann.*, **41**(4), 228–230.

Paul, F., C. Huggel and A. Kääb. 2004. Combining satellite multispectral image data and a digital elevation model for mapping debris-covered glaciers. *Remote Sens. Environ.*, **89**(4), 510–518.

Pellicciotti, F., B.W. Brock, U. Strasser, P. Burlando, M. Funk and J.G. Corripio. 2005. An enhanced temperature-index glacier melt model including shortwave radiation balance: develop-ment and testing for Haut Glacier d'Arolla, Switzerland. *J. Glaciol.*, **51**(175), 573–587.

Pellicciotti, F. and 7 others. 2008. A study of the energy balance and melt regime on Juncal Norte Glacier, semi-arid Andes of central Chile, using melt models of different complexity. *Hydrol. Process.*, **22**(19), 3980–3997.

Pellicciotti, F., M. Carenzo, J. Helbing, S. Rimkus and P. Burlando. 2009. On the role of subsurface heat conduction in glacier energy-balance modelling. *Ann. Glaciol.*, **50**(50), 16–24.

Popovnin, V.V. and A. Rozova. 2002. Influence of sub-debris thawing on ablation and runoff of the Djankuat Glacier in the Caucasus. *Nord. Hydrol.*, **33**(1), 75–94.

Purdie, J. and B. Fitzharris. 1999. Processes and rates of ice loss at the terminus of Tasman Glacier, New Zealand. *Global Planet. Change*, **22**(1–4), 79–91.

Reid, T. and N. Crout. 2008. A thermodynamic model of freshwater Antarctic lake ice. *Ecol. Model.*, **210**(3), 231–241.

Sakai, A., M. Nakawo and K. Fujita. 1998. Melt rate of ice cliffs on the Lirung Glacier, Nepal Himalayas, 1996. *Bull. Glacier Res.*, **16**, 57–66.

Sakai, A., K. Fujita and J. Kubota. 2004. Evaporation and percolation effect on melting at debris-covered Lirung Glacier, Nepal Himalayas, 1996. *Bull. Glaciol. Res.*, **21**, 9–16.

Shukla, A., R.P. Gupta and M.K. Arora. 2009. Estimation of debris cover and its temporal variation using optical satellite sensor data: a case study in Chenab basin, Himalayas. *J. Glaciol.*, **55**(191), 444–452.

Smith, G.D. 1985. *Numerical solution of partial differential equations: finite difference methods. Third edition.* Oxford, Oxford University Press.

Stokes, C.R., V. Popovin, A. Aleynikov, S.D. Gurney and M. Shahgedanova. 2007. Recent glacier retreat in the Caucasus Mountains, Russia, and associated increase in supraglacial debris cover and supra-/proglacial lake development. *Ann. Glaciol.*, **46**, 195–203.

Van den Broeke, M., P. Smeets, J. Ettema, C. van der Veen, R. van de Wal and J. Oerlemans. 2008. Partitioning of melt energy and meltwater fluxes in the ablation zone of the west Greenland ice sheet. *Cryosphere*, **2**(2), 179–189.

APPENDIX

Software

The DEB model is implemented in MATLAB® Release 2009b, copyright 1984–2009, The Mathworks, Inc. All model code is available on request from the authors.

Notes on the Newton–Raphson iteration method

The Newton–Raphson algorithm, as described in Equation (3), performs well for calculating T_s, but is occasionally unstable due to large step sizes calculated when $F'(T_s(n))$ is very small. To avoid these instabilities, a maximum step size of $|T_s(n+1) - T_s(n)| \leq 1°C$ is imposed at each stage of the algorithm. On some other occasions, the algorithm gets stuck jumping between two values on either side of a function minimum. To deal with this situation, the algorithm is always stopped if the number of steps, n, reaches 100 and the mean of the last two values is taken as the true solution for T_s.

Calculating internal debris temperatures

The heat conservation equation for the debris layer is informed by Equation (4), and takes into account the partial derivatives of debris temperature, T, with respect to time, t, and depth, z, in the form

$$\rho c \frac{\partial T(z,t)}{\partial t} = \frac{\partial}{\partial z}\left(k \frac{\partial T(z,t)}{\partial z}\right), \tag{A1}$$

where ρ, c and k are the debris density, specific heat capacity and thermal conductivity, respectively (the subscript 'd' for debris is not used in this Appendix, for clarity). For a debris layer of thickness d, we define N internal calculation layers, each with thickness $h = d/N$, such that the jth layer is at depth $z_j = jh$ ($j = 0, 1, 2, ..., N$). Similarly, for a time-step of size Δt, the mth time-step is at $t_m = m\Delta t$ ($m = 0, 1, 2, ...$). Now, to calculate temperature in the jth layer at time $m + 1$, we can integrate Equation (A1) over the intervals $[z_{j-12}, z_{j+12}]$ and $[t_m, t_{m+1}]$. By adopting the notation T_j^m for the debris temperature at time-step m in layer j, the left-hand side of Equation (A1) becomes:

$$\int_{z_{j-\frac{1}{2}}}^{z_{j+\frac{1}{2}}} \int_{t_m}^{t_{m+1}} \rho c \frac{\partial T}{\partial t}\, dz\, dt \approx h\rho c \left(T_j^{m+1} - T_j^m\right). \tag{A2}$$

Next, we define the function $X(z,t) = \partial T/\partial z$, which is calculated at a depth of z_{j+12} by applying the central difference approximation:

$$X_{j+\frac{1}{2}}^m \approx \frac{T_{j+1}^m - T_j^m}{h}. \tag{A3}$$

Now the right-hand side of Equation (A1) can be rewritten as:

$$\int_{z_{j-\frac{1}{2}}}^{z_{j+\frac{1}{2}}} \int_{t_m}^{t_{m+1}} k \frac{\partial X}{\partial z}\, dz\, dt = k \int_{t_m}^{t_{m+1}} \left(X_{j+\frac{1}{2}}^m - X_{j-\frac{1}{2}}^m\right) dt$$
$$\approx \frac{k\Delta t}{2}\left(X_{j+\frac{1}{2}}^{m+1} - X_{j-\frac{1}{2}}^{m+1} + X_{j+\frac{1}{2}}^m - X_{j-\frac{1}{2}}^m\right), \tag{A4}$$

where the time integration on the last step is solved using a trapezoidal approximation, which is sufficiently accurate for a short time-step. Finally, by combining Equations (A2) and (A4), and expanding all terms in X according to Equation (A3), we obtain the numerical scheme

$$T_j^{m+1} - T_j^m = \frac{k\Delta t}{2\rho ch^2}\left(T_{j+1}^{m+1} - 2T_j^{m+1} + T_{j-1}^{m+1}\right)$$
$$+ \frac{k\Delta t}{2\rho ch^2}\left(T_{j+1}^m - 2T_j^m + T_{j-1}^m\right), \tag{A5}$$

which shows that the change in temperature of layer j from one time-step to the next depends on temperatures in layer j and its neighbouring layers, $j - 1$ and $j + 1$, at both the new (t_{m+1}) and previous (t_m) time-steps. Equation (A5) represents a series of equations that can be written out in the Crank–Nicholson form, here using the notation of Smith (1985), with everything known on the right-hand side and everything unknown on the left:

$$T_0^{m+1} = T_s(t_{m+1})$$
$$+ b_1 T_1^{m+1} - c_1 T_2^{m+1} = d_1$$
$$- a_2 T_1^{m+1} + b_2 T_2^{m+1} - c_2 T_3^{m+1} = d_2$$
$$... = ...$$
$$- a_j T_{j-1}^{m+1} + b_j T_j^{m+1} - c_j T_{j+1}^{m+1} = d_j$$
$$... = ...$$
$$- a_{N-1} T_{N-2}^{m+1} + b_{N-1} T_{N-1}^{m+1} = d_{N-1}$$
$$T_N^{m+1} = T_f, \tag{A6}$$

where the as, bs, cs and ds are all known quantities. The top and bottom equations contain two boundary conditions for the scheme: the newly estimated debris surface temperature $T_s(t_{m+1})$ and the temperature of the debris base, which is assumed to remain at the freezing point of water, $T_f = 273.15$ K. Defining a constant $C = k\Delta t/2\rho ch^2$, Equation (A5) can similarly be rewritten with known quantities on the right and unknowns on the left:

$$- CT_{j-1}^{m+1} + (2C + 1)T_j^{m+1} - CT_{j+1}^{m+1}$$
$$= CT_{j-1}^m + (1 - 2C)T_j^m + CT_{j+1}^m. \tag{A7}$$

Comparing Equations (A6) and (A7), we infer that the required constants are

$$a_j = C$$
$$b_j = 2C + 1$$
$$c_j = C, \tag{A8}$$

for all j, where $j = 1, ..., N - 1$. The values of d_j are:

$$d_1 = CT_s(t_{m+1}) + CT_s(t_m) + (1 - 2C)T_1^m + CT_2^m$$
$$d_j = CT_{j-1}^m + (1 - 2C)T_j^m + CT_{j+1}^m \tag{A9}$$
$$d_{N-1} = 2CT_f + CT_{N-2}^m + (1 - 2C)T_{N-1}^m,$$

where the second equation applies to $j = 2, ..., N - 2$. Continuing in the notation of Smith (1985), we define two

variables A and S:

$$A_1 = b_1$$
$$A_i = b_i - \frac{a_i}{A_{i-1}} c_{i-1} \tag{A10}$$

$$S_1 = d_1$$
$$S_i = d_i + \frac{a_i}{A_{i-1}} S_{i-1}, \tag{A11}$$

where $i = 2, ..., N-1$. Finally, the debris temperature at each internal layer in the ice for the new time, t_{m+1}, can be

calculated using:

$$T_{N-1}^{m+1} = \frac{S_{N-1}}{A_{N-1}}$$
$$T_j^{m+1} = \frac{1}{A_j} \left(S_j + c_j T_{j+1} \right), \tag{A12}$$

where the calculations for the second equation must be done in reverse order, $j = N-2, N-1, ..., 2, 1$. Therefore all that is required to solve the internal debris temperature within the model is to evaluate Equations (A8–A12) in order.